INTERPOLATION ON THE CUBED SPHERE WITH SPHERICAL HARMONICS

JEAN-BAPTISTE BELLET[†], MATTHIEU BRACHET[‡], AND JEAN-PIERRE CROISILLE[†]

ABSTRACT. We consider the Lagrange interpolation with Spherical Harmonics of data located on the equiangular Cubed Sphere. A new approach based on a suitable Echelon Form of the associated Vandermonde matrix is carried out. As an outcome, a particular subspace of Spherical Harmonics is defined. This subspace possesses a particular truncation, reminiscent of the rhomboidal truncation. Numerical results show the interest of this approach in various contexts. In particular, several examples of resolution of the Poisson problem on the sphere are displayed.

Keywords: Cubed Sphere Grid - Spherical Harmonics - Spectral approximation on the sphere - Romboidal Truncation - Poisson problem on the sphere

1. INTRODUCTION

In this paper, the problem of interpolating data on the equiangular Cubed Sphere with Spherical Harmonics is considered. The equiangular Cubed Sphere is a particular spherical grid widely used to discretize problems on the sphere. For example, in numerical climatology and meteorology, it is used to support discrete unknowns with various approximations procedures, as finite volume schemes.

A standard computational approach for PDE's on the sphere is based on the spectral approximation. In this case, the discrete unknowns are expanded in a finite sum of Spherical Harmonics. The discrete PDE is obtained by collocation at the nodes of the lon-lat grid. Nonlinear terms appearing in the PDE's are classically treated by the pseudospectral method. In this approach, an important parameter is the truncation scheme (typically triangular or rhomboidal), which monitors the finite summation limits in the Spherical Harmonics series. This impacts both the convergence and the aliasing behaviour of the method.

Here we are interested to replace the lon-lat grid by the Cubed Sphere. More precisely, having selected the Cubed Sphere nodes as location for the discrete unknowns, we wish to interpolate these unknowns with a suitable set of Spherical Harmonics. This question seems open in the literature. Apart of its own interest, it seems relevant in order to shed light on important mathematical properties of the Cubed Sphere. In particular, the "approximation power" of the Cubed Sphere has been remarked in various contexts, including numerical schemes of various kinds [3, 9, 13] and spherical quadrature [10].

Our first purpose is therefore to introduce a suitable subspace of Spherical Harmonics having the "unisolvence" property when associated to the Cubed Sphere nodes. This particular Lagrange interpolation problem is treated here both from the theoretical and the computational point of view. First, we consider the existence and uniqueness of a particular set of Spherical Harmonics when restricted to the Cubed Sphere. Contrary to the case of the lon-lat grid, this subspace naturally entails the high frequency truncation scheme. The truncation here emerges as an outcome of our method, and not as a parameter to be selected. Second, a new algorithm to evaluate the Spherical Harmonics representation of a set of data defined on the Cubed Sphere is described.

Beyond its own theoretical interest, this interpolation problem is expected to serve as a suitable framework for a discrete harmonic analysis on the Cubed Sphere. This lays out the basis for systematic spectral approximations on the Cubed Sphere.

In Section 2, the background on the Cubed Sphere (abbrev. as CS) and the Spherical Harmonics (abbrev. as SH) is briefly recalled. The setup of the Lagrange interpolation problem (called "CS/SH") is described in Section 3. This involves the definition of various VanderMonde matrices. Our main Theorem in Section 4 consists in establishing a particular factorization in echelon form of a VanderMonde matrix. An important outcome is a computational algorithm, which closely follows the proof of the theorem. Finally in Section 5,

Date: April 10 2021b.

various numerical experiments and results are displayed. Some numerical results on the Poisson Problem on the sphere are given.

2. Notation

2.1. **The equiangular Cubed Sphere.** We consider the interpolation problem by Spherical Harmonics (SH) on the Cubed Sphere CS_N, $N \geq 1$ being a fixed resolution. In what follows, we assume that a Cartesian frame $\mathcal{R} = (0, i, j, k)$ is fixed. The definitions depends on this frame.

The Cubed Sphere grid CS_N is defined as the set of $6N^2 + 2$ nodes with coordinates

$$\mathrm{CS}_N = \left\{ \tfrac{1}{\sqrt{1+u_l^2+u_m^2}}(\pm 1, u_l, u_m),\ \tfrac{1}{\sqrt{1+u_l^2+u_m^2}}(u_l, \pm 1, u_m),\ \tfrac{1}{\sqrt{1+u_l^2+u_m^2}}(u_l, u_m, \pm 1) \right\} \tag{1}$$

where the u_l are equidistribued on $[-\pi/4, \pi/4]$ as

$$u_l = \tan \tfrac{l\pi}{2N}. \tag{2}$$

This equidistribution justifies the name of *equiangular* Cubed Sphere. These nodes are numbered with the index $j \in [\![1 : \bar{N}(N)]\!]$, where we denote $\bar{N}(N) = 6N^2 + 2$ (simply called $\bar{N}$ when there is no ambiguity).

$$\mathrm{CS}_N = \{\boldsymbol{x}_j,\ j \in [\![1 : \bar{N}]\!]\}. \tag{3}$$

Refer to [12] for more details and to [11] for alternative Cubed Sphere grid.

2.2. **Spherical Harmonics.** Our notation for Spherical Harmonic functions is as follows.

- The set Y_n is

$$Y_n = \mathrm{Span}\,(Y_n^m(\boldsymbol{x}),\ -n \leq m \leq n)\ n \geq 0, \tag{4}$$

  with the SH function Y_n^m is defined by

$$Y_n^m(\boldsymbol{x}) = Y_n^m(\theta, \phi) = (-1)^{|m|} \sqrt{\tfrac{(n+1/2)(n-|m|)!}{\pi(n+|m|)!}} P_n^{|m|}(\sin\theta) \times \begin{cases} \sin |m|\phi, & m < 0, \\ \frac{1}{\sqrt{2}}, & m = 0, \\ \cos m\phi, & m > 0. \end{cases} \tag{5}$$

  We denote

$$\begin{cases} \boldsymbol{x} = (\cos\theta\cos\phi, \cos\theta\sin\phi, \sin\theta) \\ \phi \in [-\pi, \pi],\ \text{azimuth or longitude}\ \text{ and } \theta \in [-\frac{\pi}{2}, \frac{\pi}{2}]\ \text{elevation or latitude.} \end{cases} \tag{6}$$

  In (5), the associated Legendre function is

$$P_n^{|m|}(t) = (-1)^{|m|}(1-t^2)^{|m|/2} \tfrac{\mathrm{d}^{|m|+n}}{\mathrm{d}t^{|m|+n}} \tfrac{1}{2^n n!}(t^2-1)^n. \tag{7}$$

- We denote $\mathcal{Y}_n$ the set of HS functions of degree less or equal to n,

$$\mathcal{Y}_n = Y_0 \oplus \cdots \oplus Y_n. \tag{8}$$

The set $(Y_n^m)_{-n \leq m \leq n}$ is an orthonormal basis of Y_n for the scalar product of $L^2(\mathbb{S}^2)$ given by

$$(f, g)_2 = \int_{\mathbb{S}^2} f(\boldsymbol{x}) g(\boldsymbol{x}) \mathrm{d}\sigma. \tag{9}$$

The infinite family $(Y_n^m)_{|m| \leq n, n \in \mathbb{N}}$ is a Hilbert basis of $L^2(\mathbb{S}^2)$. We refer to [1, 7] for more details.

3. Lagrange interpolation on the Cubed Sphere with Spherical Harmonics

3.1. **General setup.** Let $(y_j)_{1\le j\le \bar N}$ be a set of values given at the nodes $\boldsymbol{x}_j$. We are interested in finding a SH function $p(\boldsymbol{x})$ satisfying the equations

$$p(\boldsymbol{x}_j) = y_j, \quad \forall 1 \le j \le \bar N. \tag{10}$$

Problem (CS/HS)**:** *Find an integer $N' = N'(N)$ and a subspace $\mathcal{Y}'_{N'} \subset \mathcal{Y}_{N'}$, such that the interpolation problem (10) with $p \in \mathcal{Y}'_{N'}$ has a unique solution.*

Observe that the integer N' depends of N, and is part of the unknowns. In Section 4 below, we propose a constructive algorithm to solve the problem (CS/HS).

3.2. **VanderMonde matrices.** We analyse the structure of various *Vandermonde matrices* (abbreviated as VDM) associated to the problem (CS/HS).

Definition 3.1 (VanderMonde matrices)**.** Let N be the resolution of the Cubed Sphere (1) and $\bar N = 6N^2+2$ the number of nodes.

- For k fixed, the rectangular matrix A_k is the VDM matrix associated to the basis $Y_k^m, -k \le m \le k$ of the SH space Y_k, and to the nodes $\boldsymbol{x}_j \in CS_N$, is defined by

$$A_k \triangleq [Y_k^m(\boldsymbol{x}_j)]_{-k\le m\le k, 1\le j\le \bar N} \in \mathbf{R}^{(2k+1)\times \bar N}. \tag{11}$$

- For n fixed, the matrix $\boldsymbol{A}_n$ is the VDM matrix associated to the basis $(Y_k^m)_{|m|\le k\le n}$ of the space $\mathcal{Y}_n$. It is defined by

$$\boldsymbol{A}_n \triangleq \begin{bmatrix} A_0 \\ \vdots \\ A_n \end{bmatrix} \in \mathbf{R}^{(n+1)^2\times \bar N}. \tag{12}$$

Let N' be a fixed integer and $\mathcal{Y}_{N'} = Y_0 \oplus \cdots \oplus Y_{N'}$. Let $p(\boldsymbol{x})$ be the HS function with decomposition in the Legendre basis

$$\begin{aligned} p(\boldsymbol{x}) &= \sum_{0\le n\le N'} \sum_{|m|\le n} p_n^m Y_n^m(\boldsymbol{x}) \\ &= [Y_n^m(\boldsymbol{x})]^\intercal [p_n^m] \end{aligned} \tag{13}$$

The vector $[p(\boldsymbol{x}_j)]^\intercal \in \mathbf{R}^{\bar N}$ is expressed in term of the matrix $\boldsymbol{A}_{N'}$ and of the components $[p_n^m]$ by

$$[p(\boldsymbol{x}_1), \dots p(\boldsymbol{x}_{\bar N})]^\intercal = \boldsymbol{A}_{N'}^\intercal [p_n^m] \tag{14}$$

Therefore, the interpolation problem (10) is expressed with the VDM matrix $\boldsymbol{A}_{N'}$ by the system

$$\boldsymbol{A}_{N'}^\intercal [p_n^m] = \mathbf{y}, \tag{15}$$

where $\mathbf{y} = [y_1, \dots, y_{\bar N}]^\intercal$. A sufficient condition for the VDM matrix $\boldsymbol{A}_n$ to have full rank results from the following result.

Proposition 3.2 (Lemma 3.13 in [8])**.** *Let $\Omega = \{\boldsymbol{x}_j, 1 \le j \le M\} \subset \mathbb{S}^{d-1}$ be a general distribution of nodes on the d-dimensional sphere. Let*

$$\operatorname{sep}(\Omega) = \min_{j\ne l} \arccos(\boldsymbol{x}_j^\intercal \boldsymbol{x}_l) \tag{16}$$

denotes the separation distance of the nodes in Ω. The nodes are called "q-separated" if $\operatorname{sep}(\Omega) > q$. Assuming that n is such that $n > 2.5\pi d$, then the VDM matrix

$$Z_n \in \mathbf{R}^{M\times N}, \quad Z_n \triangleq \left(Y_k^l(\boldsymbol{x}_j)\right)_{l=-k\dots k, j=1,\dots M} \tag{17}$$

has full row rank M.

In the particular case where the $\boldsymbol{x}_j$ are the nodes of CS_N, we call $\operatorname{sep}(\mathrm{CS}_N)$ the separation distance on CS_N.

Corollary 3.3 (sufficient condition for $\boldsymbol{A}_n$ to have full column rank)**.** *Let $n \geq 1$ and let $0 < q_N < \mathrm{sep}(\mathrm{CS}_N)$ be such that $n > \frac{7.5\pi}{q_N}$. Then the VDM matrix $\boldsymbol{A}_n \in \mathbf{R}^{(n+1)^2 \times \bar{N}}$ has full column rank $\bar{N}$.*

Definition 3.4 (rank and "rank increment")**.** For all $n \geq 0$, the rank of $\boldsymbol{A}_n$ is denoted by r_n and the rank increment between $\boldsymbol{A}_{n-1}$ and $\boldsymbol{A}_n$ is denoted by g_n:

$$\begin{cases} r_n \triangleq \mathrm{rank}\,\boldsymbol{A}_n, n \geq 0, \\ g_n \triangleq r_n - r_{n-1}, n \geq 0, \end{cases} \tag{18}$$

with the convention $r_{-1} \triangleq 0, \quad g_0 \triangleq r_0$.

By Corollary 3.3, for n large enough, we have $\mathrm{rank}(\boldsymbol{A}_n) = \bar{N}$. This justifies the following definition

Definition 3.5 (integer $N'(N)$)**.** We call $N'(N)$ (or simply N' in case of no ambiguity), the smallest integer n such that $\boldsymbol{A}_n$ has full column rank $\bar{N}$. Equivalently, N' is defined by

$$N' = \min\{n \geq 0 \text{ such that } r_n = \bar{N}\}. \tag{19}$$

It results from Corollary 3.3 that

$$N' \leq \frac{7.5\pi}{q_N}. \tag{20}$$

Refer to Remark 5.3 for further comments on the value $\mathrm{sep}(CS_N)$.

4. Constructing a SH subspace on the Cubed Sphere

In this section we give a constructive algorithm to build a subspace $\mathcal{Y}'_{N'}$ of SH functions solving the problem (CS/HS) above. It consists in constructing a suitable factorization of the sequence of matrices $(\boldsymbol{A}_n)_{n\geq 0}$. The factorization itself will reveal both the sequence $(r_n)_{\geq 0}$ and the integer N' in (19). See also Section 5.1 below.

4.1. Echelon form of matrices.

We recall the definition of a matrix in *Column Echelon* form (abbreviated CE form).

Definition 4.1 (Column Echelon form)**.** Let $A \in \mathbf{R}^{m\times n}$ be a rectangular matrix. The matrix A is said to be in CE form, if there is some $r \in [\![1:n]\!]$ such that

- the columns $j \in [\![1:r]\!]$ are nonzero, where the index $j \mapsto i(j)$ of the first nonzero coefficient a non decreasing function. (The coefficient $A(i(j), j), 1 \leq j \leq r$, is called the *pivot* of the column j).

- the columns $j \in [\![r+1:n]\!]$ are zero.

A matrix $A \in \mathbf{R}^{m\times n}$ can be reduced in CE form using Gaussian elimination with partial pivoting on the columns. In addition, the number r of pivots represents the rank of the matrix.

In the sequel, we show that the VDM matrix $\boldsymbol{A}_n$ in (12) can be expressed in CE form by mean of suitable orthogonal matrices.

4.2. Factorization of the VDM matrix $\boldsymbol{A}_n$.

In the next theorem, we establish a particular factorization of the VanderMonde matrix $\boldsymbol{A}_n$. This factorization serves to define a computational procedure to identify a space $\mathcal{Y}'_n \subset \mathcal{Y}_n$ satisfying (10). As a byproduct, the maximal degree N' in (19) and the rank increment sequence $(g_n)_{0\leq n\leq \bar{N}}$ will be identified as well.

Recall that the VDM matrix $\boldsymbol{A}_n$ is defined by

$$\boldsymbol{A}_n \triangleq \begin{bmatrix} A_0 \\ \vdots \\ A_n \end{bmatrix} \in \mathbf{R}^{(n+1)^2\times \bar{N}}. \tag{21}$$

Theorem 4.2 (Structure of $\boldsymbol{A}_n$)**.** *Let $n \geq 0$.*
The matrix $\boldsymbol{A}_n$ can be factorized in the form

$$\boldsymbol{A}_n = \boldsymbol{U}_n \boldsymbol{E}_n \boldsymbol{V}_n^{\intercal}, \tag{22}$$

where

- *The matrices* $\boldsymbol{U}_n, \boldsymbol{V}_n$ *are orthogonal with*

$$\begin{cases} \boldsymbol{U}_n \in \mathbf{R}^{(n+1)^2\times(n+1)^2}, \\ \boldsymbol{V}_n \in \mathbf{R}^{\bar{N}\times\bar{N}}. \end{cases} \tag{23}$$

- *The matrix* $\boldsymbol{E}_n \in \mathbf{R}^{(n+1)^2\times\bar{N}}$ *has rank* r_n *and is in CE form as displayed in Fig. 1 (left panel).*

In particular, $\operatorname{rank}(E_n) = r_n$.

Proof. The proof is constructive. Therefore, in the course of it, recurrence formulas emerge, which play an important role in the computational procedure. It allows to identify both the degree N' and a suitable space $\mathcal{Y}'_{N'}$ in (10). We proceed by induction on the degree $n \geq 0$. First for $n = 0$, $Y_0^0(\boldsymbol{x}) = 1/\sqrt{4\pi}$. Therefore $\boldsymbol{A}_0 = \frac{1}{\sqrt{4\pi}}[1, 1, \ldots, 1] \in \mathbf{R}^{1\times\bar{N}}$. A SVD decomposition is expressed as $\boldsymbol{A}_0 = U_0 S_0 V_0^\intercal$ with

$$U_0 = [1],\ S_0 = [\sqrt{N/4\pi}, 0, \ldots, 0],\ V_0 = [v_1, v_2, \ldots v_{\bar{N}}] \tag{24}$$

where $V_0 \in \mathbf{R}^{\bar{N}\times\bar{N}}$ is orthogonal and $v_1 = \frac{1}{\sqrt{N}}[1, 1, \ldots, 1]^\intercal$. We set $\boldsymbol{U}_0 = U_0$, $\boldsymbol{V}_0 = V_0$ and $\boldsymbol{E}_0 = S_0$. Assume now (induction step) that the result holds for $n-1$. We have $\boldsymbol{A}_{n-1} = \boldsymbol{U}_{n-1}\boldsymbol{E}_{n-1}\boldsymbol{V}_{n-1}$ for some orthogonal matrices $\boldsymbol{U}_{n-1}$ and $\boldsymbol{V}_{n-1}$ and for $\boldsymbol{E}_{n-1}$ in CE form (see Fig. 1). Consider the matrix

$$\begin{aligned} \begin{bmatrix} \boldsymbol{U}_{n-1}^\intercal & \mathbf{0}_{n^2,2n+1} \\ \mathbf{0}_{2n+1,n^2} & \mathrm{I}_{2n+1} \end{bmatrix} \boldsymbol{A}_n \boldsymbol{V}_{n-1} &= \begin{bmatrix} \boldsymbol{U}_{n-1}^\intercal & \mathbf{0}_{n^2,2n+1} \\ \mathbf{0}_{2n+1,n^2} & \mathrm{I}_{2n+1} \end{bmatrix} \begin{bmatrix} \boldsymbol{A}_{n-1} \\ A_n \end{bmatrix} \boldsymbol{V}_{n-1} \\ &= \begin{bmatrix} \boldsymbol{U}_{n-1}^\intercal & \mathbf{0}_{n^2,2n+1} \\ \mathbf{0}_{2n+1,n^2} & \mathrm{I}_{2n+1} \end{bmatrix} \begin{bmatrix} \boldsymbol{U}_{n-1}\boldsymbol{E}_{n-1}\boldsymbol{V}_{n-1}^\intercal \\ A_n \end{bmatrix} \boldsymbol{V}_{n-1} \\ &= \begin{bmatrix} \boldsymbol{E}_{n-1} \\ A_n \boldsymbol{V}_{n-1} \end{bmatrix}. \end{aligned} \tag{25}$$

Using the CE form of $\boldsymbol{E}_{n-1}$ shown in Fig. 1, we have

$$\begin{bmatrix} \boldsymbol{E}_{n-1} \\ A_n \boldsymbol{V}_{n-1} \end{bmatrix} = \begin{bmatrix} \boldsymbol{E}_{n-1}([\![1:n^2]\!], [\![1:r_{n-1}]\!]) & \mathbf{0}([\![1:n^2]\!], [\![r_{n-1}+1, \bar{N}]\!]) \\ A_n \boldsymbol{V}_{n-1}([\![1:\bar{N}]\!], [\![1:r_{n-1}]\!]) & A_n \boldsymbol{V}_{n-1}([\![1:\bar{N}]\!], [\![r_{n-1}+1:\bar{N}]\!]) \end{bmatrix}. \tag{26}$$

The orthogonal matrices U_n, V_n and the block diagonal matrix S_n are defined by the SVD of the block in position $(2, 2)$ in (26)

$$A_n \boldsymbol{V}_{n-1}([\![1:\bar{N}]\!], [\![r_{n-1}+1:\bar{N}]\!]) = U_n S_n V_n^\intercal. \tag{27}$$

We have that $\operatorname{rank} A_{n-1} = \operatorname{rank} E_{n-1}$. Therefore, using (18) and (26), it turns out that

$$\operatorname{rank} S_n = g_n. \tag{28}$$

By definition of the SVD, U_n and V_n are orthogonal, whereas S_n is diagonal, with nonnegative and nonincreasing values along the diagonal. This gives that (25) can be expressed as

$$\begin{bmatrix} \boldsymbol{U}_{n-1}^\intercal & \mathbf{0}_{n^2,2n+1} \\ \mathbf{0}_{2n+1,n^2} & \mathrm{I}_{2n+1} \end{bmatrix} \boldsymbol{A}_n \boldsymbol{V}_{n-1} = \begin{bmatrix} \boldsymbol{E}_{n-1}([\![1:n^2]\!], [\![1:r_{n-1}]\!]) & \mathbf{0}([\![1:n^2]\!], [\![r_{n-1}+1, \bar{N}]\!]) \\ A_n \boldsymbol{V}_{n-1}([\![1:\bar{N}]\!], [\![1:r_{n-1}]\!]) & U_n S_n V_n^\intercal \end{bmatrix}. \tag{29}$$

Multiplying (29) on the left by $\begin{bmatrix} \mathrm{I}_{n^2} & \mathbf{0}_{n^2,2n+1} \\ \mathbf{0}_{2n+1,n^2} & U_n^\intercal \end{bmatrix}$, and on the right by $\begin{bmatrix} \mathrm{I}_{n^2} & \mathbf{0}_{n^2,2n+1} \\ \mathbf{0}_{2n+1,n^2} & V_n \end{bmatrix}$ yields

$$\begin{bmatrix} \boldsymbol{U}_{n-1}^\intercal & \mathbf{0}_{n^2,2n+1} \\ \mathbf{0}_{2n+1,n^2} & U_n^\intercal \end{bmatrix} \boldsymbol{A}_n \boldsymbol{V}_{n-1} \begin{bmatrix} \mathrm{I}_{n^2}^\intercal & \mathbf{0}_{n^2,2n+1} \\ \mathbf{0}_{2n+1,n^2} & V_n \end{bmatrix} = \underbrace{\begin{bmatrix} \boldsymbol{E}_{n-1}([\![1:n^2]\!], [\![1:r_{n-1}]\!]) & \mathbf{0}([\![1:n^2]\!], [\![r_{n-1}+1, \bar{N}]\!]) \\ U_n^\intercal A_n \boldsymbol{V}_{n-1}([\![1:n^2]\!], [\![1:r_{n-1}]\!]) & S_n \end{bmatrix}}_{\boldsymbol{E}_n}. \tag{30}$$

Define the matrices $\boldsymbol{U}_n$ and $\boldsymbol{V}_n$ in terms of the orthogonal matrices $\boldsymbol{U}_{n-1}$, $\boldsymbol{V}_{n-1}$, U_n and V_n by

$$\begin{cases} \boldsymbol{U}_n = \begin{bmatrix} \boldsymbol{U}_{n-1} & \mathbf{0}_{n^2,2n+1} \\ \mathbf{0}_{2n+1,n^2} & U_n \end{bmatrix}, \\ \boldsymbol{V}_n = \boldsymbol{V}_{n-1} \begin{bmatrix} \mathrm{I}_{n^2} & 0 \\ 0 & V_n \end{bmatrix}. \end{cases} \tag{31}$$

The matrices $\boldsymbol{U}_n$ and $\boldsymbol{V}_n$ are orthogonal and satisfy $\boldsymbol{U}_n\boldsymbol{A}_n\boldsymbol{V}_n = \boldsymbol{E}_n$, which is equivalent to (22). Furthermore it turns out that the matrix $\boldsymbol{E}_n$ defined in (30) is in CE form. In fact we have $r_n = \operatorname{rank} E_n = r_{n-1} + \operatorname{rank} S_n$. This proves that $\operatorname{rank} S_n = g_n$ and that E_n has the shape shown in Fig. **??**. □

As already mentioned, the steps in the proof of the Theorem 4.2 can be turned into a computational algorithm, with a loop over the integer n, as follows

Algorithm 4.3. *While $r_n < \bar{N} = 6N^2 + 2$, do for $n \geq 0$,*
1. *compute the matrix A_n;*
2. *compute the matrices U_n, S_n, V_n, by SVD of the matrix in (27) (24 for $n = 0$);*
3. *assemble the matrices $\boldsymbol{E}_n$, $\boldsymbol{V}_n$ and $\boldsymbol{U}_n$ by (30-31).*
4. *compute the rank increment g_n by (28), and the rank $r_n = r_{n-1} + g_n$.*

End While

5. *The algorithm exits exactly when $r_n = \bar{N}$.*

Corollary 4.4. *Let $n \geq 0$.*
(i) The columns of $\boldsymbol{V}_n([\![1 : \bar{N}]\!], [\![r_n + 1 : \bar{N}]\!])$ are an orthonormal basis of $\operatorname{Ker} \boldsymbol{A}_n$.
(ii) The columns of $U_n([\![1 : \bar{N}]\!], [\![1 : g_n]\!])$ are an orthonormal basis of $\operatorname{Ran}(A_n\boldsymbol{V}_{n-1}([\![1 : \bar{N}]\!], [\![r_{n-1}+1 : \bar{N}]\!]))$.

We consider now the functional interpretation of the algorithm (4.3). It allows to define a particular Spherical Harmonic subspace, which provide a suitable answer to the problem (P). First we define the functions $u_n^i(\boldsymbol{x})$ as follows.

Definition 4.5 (Functions u_n^i)**.** For all $0 \leq n \leq N'$ and $1 \leq i \leq 2n+1$, the Spherical Harmonics $u_n^i(\boldsymbol{x}) \in Y_n$ is defined from the column vectors of the matrix U_n by

$$u_n^i(\boldsymbol{x}) := [Y_n^m(\boldsymbol{x})]_{-n\leq m\leq n}^{\intercal} U_n([\![1 : \bar{N}]\!], i). \tag{32}$$

The u_n^i form on orthonormal family of Y_n.

Definition 4.6 (SH spaces Y_n' and $\mathcal{Y}_n'$)**.** (i) For all $0 \leq n \leq N'$, we call Y_n' and Y_n'' the spaces defined by

$$Y_n' \triangleq \operatorname{Span}\{u_n^i, 1 \leq i \leq g_n\} \subset Y_n, \quad Y_n'' \triangleq \operatorname{Span}\{u_n^i, g_n + 1 \leq i \leq 2n+1\} \tag{33}$$

and

$$Y_n = Y_n' \overset{\perp}{\oplus} Y_n''. \tag{34}$$

(ii) The SH subspace $\mathcal{Y}_{N'}'$is defined by

$$\mathcal{Y}_{N'}' \triangleq Y_0' \oplus \cdots \oplus Y_{N'}' = \operatorname{Span}\{u_n^i, 1 \leq i \leq g_n, 0 \leq n \leq N'\}. \tag{35}$$

The space Y_n'' is the space of SH functions of degree n which are "incorrectly represented" on the Cubed Sphere CS_N. This means that their restriction to CS_N coincides with the restriction of a SH function of smaller degree. This is expressed as follows

Corollary 4.7 (Interpretation of the space Y_n'')**.** *For $n \geq 1$, the SH subspace Y_n'' satisfies*

$$Y_n'' = \{f \in Y_n : f|_{\mathrm{CS}_N} \in \operatorname{Ran} \boldsymbol{A}_{n-1}^{\intercal}\} = \{f \in Y_n : \exists g \in Y_0 \oplus \cdots \oplus Y_{n-1}, f|_{\mathrm{CS}_N} = g|_{\mathrm{CS}_N}\}.$$

Proof. Let $\boldsymbol{\Pi}_{\operatorname{Ker} \boldsymbol{A}_{n-1}}$, (resp. $\boldsymbol{\Pi}_{\operatorname{Ran} \boldsymbol{A}_{n-1}^{\intercal}}$) be the matrix of the orthogonal projection on $\operatorname{Ker} \boldsymbol{A}_{n-1}$, (resp. on $\operatorname{Ran} \boldsymbol{A}_{n-1}^{\intercal}$). Then the columns of $\boldsymbol{V}_{n-1}([\![1 : \bar{N}]\!], [\![r_{n-1} + 1 : \bar{N}]\!])$ form an orthonormal basis of $\operatorname{Ker} \boldsymbol{A}_{n-1}$. Similarly, the columns of $U_n([\![1 : \bar{N}]\!], [\![1 : g_n]\!])$ form an orthonormal basis of the space $\operatorname{Ran} A_n\boldsymbol{V}_{n-1}([\![1 : \bar{N}]\!], [\![r_{n-1} + 1 : \bar{N}]\!])$. Therefore, the columns of $U_n([\![1 : \bar{N}]\!], [\![1 : g_n]\!])$ form an orthonormal basis of the space $\operatorname{Ran}(A_n\boldsymbol{\Pi}_{\operatorname{Ker} \boldsymbol{A}_{n-1}}) = \Big(\operatorname{Ker}(\mathrm{I} - \boldsymbol{\Pi}_{\operatorname{Ran} \boldsymbol{A}_{n-1}^{\intercal}})A_n^{\intercal}\Big)^{\perp}$. This space represents the Spherical Harmonics of degree n with restriction to CS_N are in $\operatorname{Ran} \boldsymbol{A}_{n-1}^{\intercal}$. This means that when restricted to CS_N, they coincide with Spherical Harmonics of lower degree. □

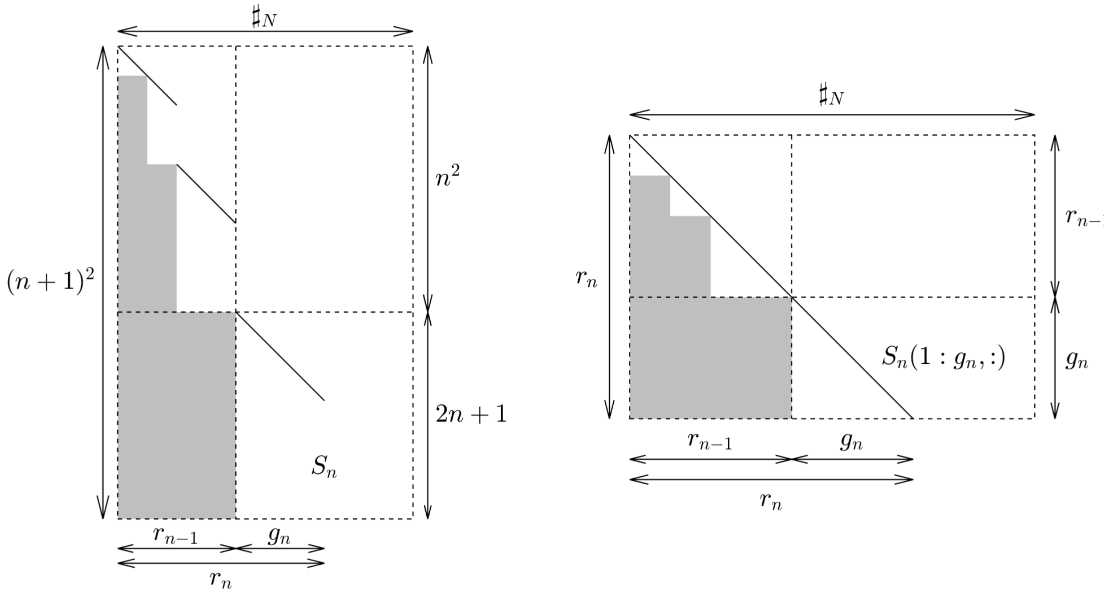

FIGURE 1. Left panel: the VDM $\boldsymbol{A}_n$ is equivalent to the column echelon matrix $\boldsymbol{E}_n$, whose shape is represented on the left. Right panel: elimination of redundant lines in $\boldsymbol{E}_n$ results in the lower triangular matrix $\boldsymbol{L}_n$, displayed on the right.

Remark 4.8. In [6, p. 602], a method is considered to numerically identify the subspace $\operatorname{Ker} M_1 \cap \operatorname{Ker} M_2$, where M_1 and M_2 are two matrices. The following SVDs are evaluated

$$\begin{cases} M_1 = U_1 S_1 V_1, \\ M_2 V_1 = U_2 S_2 V_2 \end{cases} \tag{36}$$

The space $\operatorname{Ker} M_1 \cap \operatorname{Ker} M_2$ is deduced from the knowledge of the matrices S_1, V_1 and S_2, V_2. The factorization in (25) in our approach uses a similar idea. However, a first difference is that our method uses (36) iteratively and not just once. Second, our goal is to identify an range subspace and not a kernel. Indeed, at step n, the orthonormal basis $U_n([\![1:\bar{N}]\!],[\![1:g_n]\!])$ of $\operatorname{Ran} A_n \boldsymbol{V}_{n-1}([\![1:\bar{N}]\!],[\![r_{n-1}+1:\bar{N}]\!])$ is stored, since it defines the orthonormal basis $(u_n^i)_{1\le i\le g_n}$ of $Y_n' \subset \mathcal{Y}_{N'}'$.

4.3. **Row compression.** Consider again the factorization (30). It is expressed as

$$\boldsymbol{U}_n^{\intercal} \boldsymbol{A}_n = \boldsymbol{E}_n \boldsymbol{V}_n. \tag{37}$$

We perform a row compression by eliminating redundant rows in (37). This leads to define the matrices $\tilde{\boldsymbol{U}}_n \in \mathbf{R}^{(n+1)^2 \times r_n}$ and $\boldsymbol{L}_n \in \mathbf{R}^{r_n \times \bar{N}}$ by

$$\begin{aligned} \tilde{\boldsymbol{U}}_n &= \begin{bmatrix} U_0([\![1:1]\!],[\![1:g_0]\!]) & & \\ & \ddots & \\ & & U_n([\![1:2n+1]\!],[\![1:g_n]\!]) \end{bmatrix}, \\ \boldsymbol{L}_n &= \begin{bmatrix} \mathrm{I}_1([\![1:g_0]\!],[\![1:1]\!]) & & \\ & \ddots & \\ & & \mathrm{I}_{2n+1}([\![1:g_n]\!],[\![1:2n+1]\!]) \end{bmatrix} \boldsymbol{E}_n. \end{aligned} \tag{38}$$

The matrix $\boldsymbol{L}_n$ in (38) is lower triangular. It contains the pivot rows of the column echelon matrix $\boldsymbol{E}_n$. Doing so, the rows of S_k, $k \le n$, with nonzero singular values are conserved and the zero rows of S_k are eliminated. This is summarized in the following

Corollary 4.9. *(i) The matrix $\tilde{\boldsymbol{U}}_n^\intercal \boldsymbol{A}_n$ admits the following LQ factorization*

$$\tilde{\boldsymbol{U}}_n^\intercal \boldsymbol{A}_n = \boldsymbol{L}_n \boldsymbol{V}_n^\intercal, \tag{39}$$

where the matrix $\boldsymbol{L}_n$ is lower triangular and has full row rank with $\operatorname{rank} \boldsymbol{L}_n = r_n$*, and $\tilde{\boldsymbol{U}}_n^\intercal \tilde{\boldsymbol{U}}_n = I_{r_n}$.*

(ii) In particular for the degree $n = N'$ in (19), we have $r_{N'} = \bar{N}$ and the matrix $\boldsymbol{A}_{N'}$ has full column rank. The factorization (39) of $\boldsymbol{A}_{N'}$

$$\tilde{\boldsymbol{U}}_{N'}^\intercal \boldsymbol{A}_{N'} = \boldsymbol{L}_{N'} \boldsymbol{V}_{N'}^\intercal \tag{40}$$

is such that the lower triangular matrix $\boldsymbol{L}_{N'} \in \mathbf{R}^{\bar{N} \times \bar{N}}$ is non singular.

The compressed factorization (40) now gives a solution to the interpolation problem (P).

Corollary 4.10 (Solution to Problem (CS/HS))**.** *The space $\mathcal{Y}'_{N'}$ is unisolvent for the Lagrange interpolation problem (CS/HS).*

$$\forall \boldsymbol{y} \in \mathbf{R}^{\bar{N}},\ \exists! u \in \mathcal{Y}'_{N'}, \quad u(\boldsymbol{x}_j) = y_j, \ \ j = 1, \ldots, \bar{N}. \tag{41}$$

The SH function $u(\boldsymbol{x})$ is expressed in the basis Y_n^m by

$$\begin{cases} u(\boldsymbol{x}) = [Y_n^m(\boldsymbol{x})]_{|m| \le n \le N'}^\intercal \tilde{\boldsymbol{U}}_{\mathrm{N}'} \boldsymbol{\alpha}, \\ \quad \boldsymbol{\alpha} = (\boldsymbol{L}_{\mathrm{N}'}^\intercal)^{-1} \boldsymbol{L}_{\mathrm{N}'}^\intercal \boldsymbol{y}. \end{cases} \tag{42}$$

The vector $\boldsymbol{\alpha}$ is obtained by backward substitution in the upper triangular system $\boldsymbol{L}_{N'}^\intercal \boldsymbol{\alpha} = \boldsymbol{V}_{N'}^\intercal \boldsymbol{y}$.

Proof. Let $u \in \mathcal{Y}'_{N'}$. There exists a unique family of $\bar{N}$ reals, $\boldsymbol{\alpha} = (\alpha_n^i)_{0 \le n \le N', 1 \le i \le g_n}$, such that

$$u(\cdot) = \sum_{0 \le n \le N'} \sum_{1 \le i \le g_n} \alpha_n^i u_n^i(\cdot) = [Y_n^m(\cdot)]_{|m| \le n \le N'}^\intercal \tilde{\boldsymbol{U}}_{\mathrm{N}'} \boldsymbol{\alpha}. \tag{43}$$

By the Theorem 4.9, we have

$$[u(\boldsymbol{x}_j)]_{1 \le j \le \bar{N}} = \boldsymbol{A}_{N'}^\intercal \tilde{\boldsymbol{U}}_{N'} \boldsymbol{\alpha} = \boldsymbol{V}_{N'} \boldsymbol{L}_{N'}^\intercal \boldsymbol{\alpha}, \tag{44}$$

where $\boldsymbol{V}_{N'}$ is orthogonal, and $\boldsymbol{L}_{N'}$ is lower triangular and nonsingular. Therefore the function $u(\boldsymbol{x})$ is a SH function interpolating the data $\boldsymbol{y} \in \mathbf{R}^{\bar{N}}$ on CS_N if and only if the vector $\boldsymbol{\alpha}$ satifies $\boldsymbol{V}_{N'} \boldsymbol{L}_{N'}^\intercal \boldsymbol{\alpha} = \boldsymbol{y}$, which is equivalent to $\boldsymbol{\alpha} = (\boldsymbol{L}_{\mathrm{N}'}^\intercal)^{-1} \boldsymbol{V}_{\mathrm{N}'}^\intercal \boldsymbol{y}$. □

5. Numerical results

5.1. **Numerical estimate of the rank increment.** Let $N \ge 0$ be the integer representing the accuracy of the Cubed Sphere CS_N. The Corollary 3.3 asserts that the algorithm (4.3) necessarily exits after a finite number of iterations on n with exit index $n = N'$, defined in (19). Regarding the rank increment g_n, the Theorem 4.2 shows that $g_n = \operatorname{rank} S_n$ is the number of nonzero singular values of S_n, see (28). Thus g_n is numerically estimated by some thresholding of the diagonal of S_n. This kind of thresholding is commonly used to numerically determine the rank of a given matrix by using the SVD . Here, we have used such a rank evaluation to infer the value $\operatorname{rank}(\boldsymbol{A}_n) - \operatorname{rank}(\boldsymbol{A}_{n-1})$. This value has been systematically tabulated with matlab. Table 1 reports the rank increment in $\boldsymbol{A}_n$ for N increasing from $N = 1$ (Cubed Sphere with 8 nodes) to $N = 6$ (Cubed Sphere with 218 nodes) . This has led to the following claim.

Claim 5.1. *(1) $\boldsymbol{A}_{2N-1}$ has full row rank. Equivalently, $r_{2N-1} = 4N^2$.*

(2) $\boldsymbol{A}_{3N}$ has full column rank. Equivalently, $r_{3N} = \bar{N}$.

(3) The sequence of rank increments g_n in (18) is numerically observed as given by

$$g_0 = 1, \quad g_n = \begin{cases} 2n+1, & 1 \le n \le 2N-1, \\ 4(3N-n)-2, & 2N \le n \le 3N-2, \\ 3, & n = 3N-1, \\ 1, & n = 3N. \end{cases}$$

---

[0]LQ factorization is identical to QR factorization up to transposition

[0]this is the principle behind the method `rank` in matlab

From now on, if not otherwise mentioned, the Claim 5.1 will be used to further perform numerical approximations. In particular we assume that $r_{2N-1} = 4N^2$ for $n = 2N-1$, and $r_{3N} = \bar{N} = 6N^2+2$ for $n = 3N$.

	0	1	2	3	4	5	6	7	8	9	10	11	12	13	14	15	16	17	18
1	1	3	3	1															
2	1	3	5	7	6	3	1												
3	1	3	5	7	9	11	10	6	3	1									
4	1	3	5	7	9	11	13	15	14	10	6	3	1						
5	1	3	5	7	9	11	13	15	17	19	18	14	10	6	3	1			
6	1	3	5	7	9	11	13	15	17	19	21	23	22	18	14	10	6	3	1

TABLE 1. Numerically evaluated rank increment g_n of the VanderMonde matrix $\boldsymbol{A}_n$, for $1 \leq N \leq 6$ (row), $0 \leq n \leq 3N$ (column). The matlab routine `rank` has been used.

Some consequences of the Claim (5.1) are as follows

(1) The smallest $n \geq 0$ such that $r_n = \bar{N}$ is

$$N' = 3N. \tag{45}$$

(2) For every $0 \leq n \leq 2N-1$, $Y'_n = Y_n$. In particular, the unisolvent space $\mathcal{Y}'_{3N}$ contains all Spherical Harmonics of degree $n < 2N$. We have $Y_0 \oplus \cdots \oplus Y_{2N-1} \subset \mathcal{Y}'{}_{3N}$. We call

$$\mathcal{Y}'_a = Y_0 \oplus \cdots \oplus Y_{2N-1}. \tag{46}$$

(3) For all $2N \leq n \leq 3N$, $Y'_n \subsetneq Y_n$. There exists a SH of degree n, $f \in Y_n$, such that $f \notin \mathcal{Y}'_{3N}$. We call

$$\mathcal{Y}'_b = Y'_{2N} \oplus \cdots \oplus Y'_{3N}. \tag{47}$$

In summary, assuming that the Claim 5.1 holds, the Spherical Harmonic subspace attached to the Cubed Sphere CS_N by the analysis above is the space $\mathcal{Y}'_{3N}$. It is decomposed as

$$\mathcal{Y}'_{3N} = \mathcal{Y}'_a \oplus \mathcal{Y}'_b. \tag{48}$$

As a corollary, we have that for all $n > 3N$ and $f \in Y_n$, there exists $u \in \mathcal{Y}'_{3N}$ such that $f|_{\mathrm{CS}_N} = u|_{\mathrm{CS}_N}$.

Remark 5.2. A proof of Claim 5.1 is open for the moment.

Remark 5.3. In (20), an upper bound of N' has been proved to be

$$N' \leq \lceil \tfrac{7.5\pi}{(1-\epsilon)\,\mathrm{sep}(\mathrm{CS}_N)} \rceil, \tag{49}$$

where $0 < \epsilon < 1$ is a small number. One may wonder how (49) compares to the value $N' = 3N$ in (45). The analysis in [2] has etablished that the shortest geodesic distance $\mathrm{sep}(\mathrm{CS}_N)$ is realized for any short arc around the center of any edge on the Cubed Sphere. Expressing this distance in terms of the Cubed Sphere step angle $\pi/2N$ (equatorial grid size), it turns out that

$$\mathrm{sep}(\mathrm{CS}_N) \sim \frac{\sqrt{2}}{2}\frac{\pi}{2N}.$$

A straightforward consequence is that the upper bound above is bounded by

$$\tfrac{5\sqrt{2}}{1-\epsilon}N' \quad \approx 7.07N', \tag{50}$$

which is a significantly larger value than N'.

5.2. **Truncation analysis.** Approximating functions on the sphere is commonly obtained with a truncated Spherical Harmonic series. A function $\boldsymbol{x} \in \mathbb{S}_2 \mapsto f(\boldsymbol{x})$ is expanded as

$$f(\lambda, \theta) = \sum_{n=0}^{+\infty} \sum_{|m| \le n} f_n^m Y_n^m(\lambda, \theta) \tag{51}$$

or equivalently

$$f(\lambda, \theta) = \sum_{|m|=0}^{+\infty} \sum_{n=|m|}^{+\infty} f_n^m Y_n^m(\lambda, \theta) \tag{52}$$

A first truncation scheme is the *triangular* scheme. It consists in defining $f_T \simeq f$ by the finite sum

$$f_T(\lambda, \theta) = \sum_{n=0}^{N_T} \sum_{|m| \le \min(n, M_T)} f_n^m Y_n^m(\lambda, \theta). \tag{53}$$

Here M_T, N_T are parameters defining the truncation.

A second truncation is the *rhomboidal* scheme. We define $f_R \simeq f$ by

$$f_R(\lambda, \theta) = \sum_{|m| \le M_R} \sum_{n=m}^{m+N_R} f_n^m Y_n^m(\lambda, \theta). \tag{54}$$

Both truncations are represented in Fig 2.

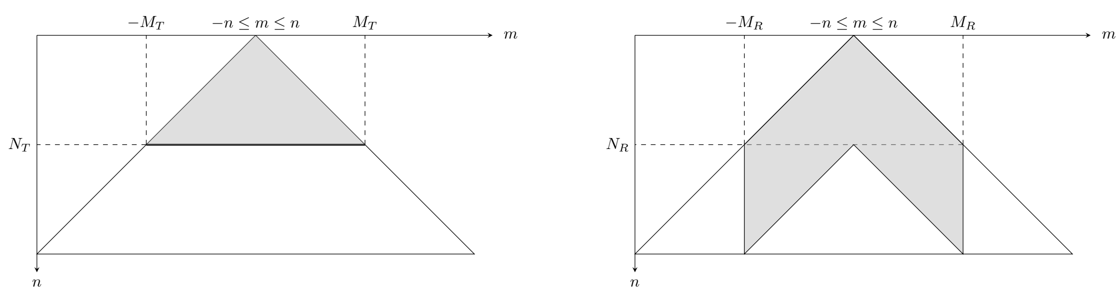

FIGURE 2. Left panel: Triangular truncation with parameters M_T and N_T. Right panel: Rhomboidal truncation with parameters M_R and N_R.

In [5] the two truncations are compared in the context of ocean numerical simulations in the case $M_T = N_T$ and $M_R = N_R$.

Here we are interested to identify which truncation is related to the approximation with the space $\mathcal{Y}'_{3N}$ in (48). In our case, there is no additional parameter to choose. The truncation, which necessarily occurs, automatically emerges from the relations (41-45).

The approximation space $\mathcal{Y}'_{3N}$ in (48) is decomposed as

$$\mathcal{Y}'_{3N} = \mathcal{Y}'_a \oplus \mathcal{Y}'_b. \tag{55}$$

Consider a given function $Y_n^m(\boldsymbol{x})$, $n \ge 0$, $|m| \le n$. The truncation scheme of the space $\mathcal{Y}'_{3N}$ is evaluated by using the least square value

$$d(Y_n^m, \mathcal{Y}'_{3N}) \triangleq \|Y_n^m - \Pi_{\mathcal{Y}'_{3N}} Y_n^m\|_2, \tag{56}$$

where $\Pi_{\mathcal{Y}'_{3N}} Y_n^m \in \mathcal{Y}'_{3N}$ stands for the orthogonal projection of Y_m^n on $\mathcal{Y}'_{3N}$. They are three cases

(1) $n < 2N$. In this case, $d(Y_n^m, \mathcal{Y}'_{3N}) = 0$. This means that $Y_m^n \in \mathcal{Y}'_a \subset \mathcal{Y}'_{3N}$.
(2) $n > 3N$. In this case, $d(Y_n^m, \mathcal{Y}'_{3N}) = 1$. This means that Y_n^m is orthogonal to $\mathcal{Y}'_{3N}$.
(3) $2N \le n \le 3N$. This is the region where the truncation occurs. This case is analyzed below.

The orthogonal projector on $\mathcal{Y}'_{3N}$, (resp. on $(\mathcal{Y}'_{3N})^{\perp}$), is represented by the matrix $\tilde{\boldsymbol{U}}_{3N}\tilde{\boldsymbol{U}}_{3N}^{\intercal}$, (resp. $\mathrm{I}-\tilde{\boldsymbol{U}}_{3N}\tilde{\boldsymbol{U}}_{3N}^{\intercal}$). We have

$$d(Y_n^m, \mathcal{Y}'_{3N}) = \min_j \|c_j(I - \tilde{\boldsymbol{U}}_{3N}\tilde{\boldsymbol{U}}_{3N}^{\intercal})\|_2 \tag{57}$$

where $c_j(M)$ stands for the column j of the matrix M. In Table 2, the distance $d(Y_n^m, \mathcal{Y}'_{3N})$ is reported in the case of the Cubed Sphere CS_2, $(N = 2)$. The results are in conformity with the case (1) above, where $\mathcal{Y}'_1 = \oplus_{n\leq 2N-1} Y_n \subset \mathcal{Y}'_{3N}$. The figures in Table 2 are reported in grayscale in Fig. 3 (top-left panel). The same results for $N = 4, 8, 16, 32$ are reported in the same fashion in the left side in Fig. 3. As can be observed, some *rhomboidal* pattern emerges for the case (3) (case $2N \leq n \leq 3N$). Two regimes of (n, m) appear

- Y_n^m is accurately approximated by the space $\mathcal{Y}'_{3N}$ if $M_n \leq |m| \leq 2N$, where $n \mapsto M_n$ is some increasing function.
- Y_n^m is orthogonal to the approximation space $\mathcal{Y}'_{3N}$ for $|m| > 2N$. This corresponds to high values for n and m.

5.3. **SVD factorization of the VDM matrix $\boldsymbol{A}_{N'}$.** In Section 4.1, a particular echelon form has been used as a building block to obtain a factorization of Vandermonde matrices. One may wonder how this compares to the more standard SVD factorization. Here we consider the alternative of using the SVD decomposition of the full VDM matrix $\boldsymbol{A}_{N'}$ in (40)

$$\boldsymbol{U}_{\mathrm{SVD}}^{\intercal}\boldsymbol{A}_{N'} = \boldsymbol{S}_{\mathrm{SVD}}\boldsymbol{V}_{\mathrm{SVD}}^{\intercal}.$$

This factor form gives that the matrix $\boldsymbol{U}_{\mathrm{SVD}} \in \mathbf{R}^{(N'+1)^2\times\bar{N}}$ contains an orthonormal basis of Ran $\boldsymbol{A}_{N'}$. The matrix $\boldsymbol{V}_{\mathrm{SVD}} \in \mathbf{R}^{\bar{N}\times\bar{N}}$ is orthogonal, and $\boldsymbol{S}_{\mathrm{SVD}} \in \mathbf{R}^{\bar{N}\times\bar{N}}$ is diagonal, nonsingular and has the positive singular values of $\boldsymbol{A}_{N'}$ on the diagonal. Suppose that, according to Claim 5.1, it holds that $N' = 3N$. Then, an approximation space $\mathcal{Y}'_{\mathrm{SVD}}$ is deduced from the columns of $\boldsymbol{U}_{\mathrm{SVD}}$. This space is a priori different from the space $\mathcal{Y}'_{3N}$ in (48). The interpolating function associated to the set of data $\boldsymbol{y} \in \mathbf{R}^{\bar{N}}$ is $u_{\mathrm{SVD}}(\boldsymbol{x})$ given by

$$u_{\mathrm{SVD}}(\boldsymbol{x}) = [Y_n^m(\boldsymbol{x})]_{|m|\leq n\leq 3N}^{\intercal}(\boldsymbol{A}_{3N}^{\intercal})^{\dagger}\boldsymbol{y}, \quad \text{with} \quad (\boldsymbol{A}_{3N}^{\intercal})^{\dagger} \triangleq \boldsymbol{U}_{\mathrm{SVD}}\boldsymbol{S}_{\mathrm{SVD}}^{-1}\boldsymbol{V}_{\mathrm{SVD}}^{\intercal}.$$

Here, $(\boldsymbol{A}_{3N}^{\intercal})^{\dagger}$ is the Moore-Penrose inverse $\boldsymbol{A}_{3N}^{\intercal}$.

We now comment on how the two spaces $\mathcal{Y}'_{3N}$ and $\mathcal{Y}'_{\mathrm{SVD}}$ compare in terms of approximation power. Table 3, is the counterpart of Table $\mathcal{Y}'_{3N}$ when replacing the space $\mathcal{Y}'_{3N}$ by the space $\mathcal{Y}'_{\mathrm{SVD}}$. Similarly, in Fig. 3, the right column is the counterpart of the left column. As can be observed, the truncation pattern is different for $\mathcal{Y}'_{3N}$ and $\mathcal{Y}'_{\mathrm{SVD}}$: when using $\mathcal{Y}'_{\mathrm{SVD}}$ the nonzero values (56) are smaller. But the proportion of the well represented Spherical Harmonics is also smaller. Notice nonzero values (56) in the region $N \leq n \leq 2N$. Overall, the space $\mathcal{Y}'_{\mathrm{SVD}}$ has less approximation power than $\mathcal{Y}'_{3N}$.

Table 4 reports a repartition analysis of the distance values (57) when using each subspace, $\mathcal{Y}'_{\mathrm{SVD}}$ and$\mathcal{Y}'_{3N}$. At least 25% of the $Y_n^m, n \leq 3N$ are in the space $\mathcal{Y}'_{3N}$. And at least 25% are almost orthogonal to $\mathcal{Y}'_{3N}$. The interquartile $Q_3 - Q_1$ and the standard deviation indicate that the distances are less dispersed in the SVD approach. The first quartile in the SVD case is larger than the median in the echelon case. In particular a larger proportion of $Y_n^m, n \leq 3N$, is accurately interpolated in $\mathcal{Y}'_{3N}$ than in $\mathcal{Y}'_{\mathrm{SVD}}$. Finally, the observed minimum value $3.8 \cdot 10^{-4}$ for the SVD approach with $N = 4$ indicates that none of the Y_n^m belongs to the space $\mathcal{Y}'_{\mathrm{SVD}}$. Moreover, the median $1.4 \cdot 10^{-3}$ $(N = 32)$ shows that half of the $Y_n^m, n \leq 3N$, are well represented in $\mathcal{Y}'_{3N}$. Finally we plot the histograms of the distances for $N = 32$ in Fig. 4. Again, these histograms support the preference to the subspace $\mathcal{Y}'_{3N}$ compared to $\mathcal{Y}'_{\mathrm{SVD}}$. The picture is as follows. Either Y_n^m almost belongs to $\mathcal{Y}'_{3N}$, either Y_n^m is almost orthogonal to $\mathcal{Y}'_{3N}$. And more that 50% of the Y_n^m almost belong to $\mathcal{Y}'_{3N}$, whereas less than 15% are close to $\mathcal{Y}'_{\mathrm{SVD}}$.

In conclusion, the incremental approach in Algorithm 4.3 has led to associate the approximation space $\mathcal{Y}'_{3N}$ to the grid CS_N. This space displays a rhomboidal like truncation in the range $2N \leq n \leq 3N$. In terms of approximation power, this space seems more promising than the space $\mathcal{Y}'_{\mathrm{SVD}}$ This is particularly true regarding the inclusion of a SH Legendre subspace as large as possible in the approximation space.

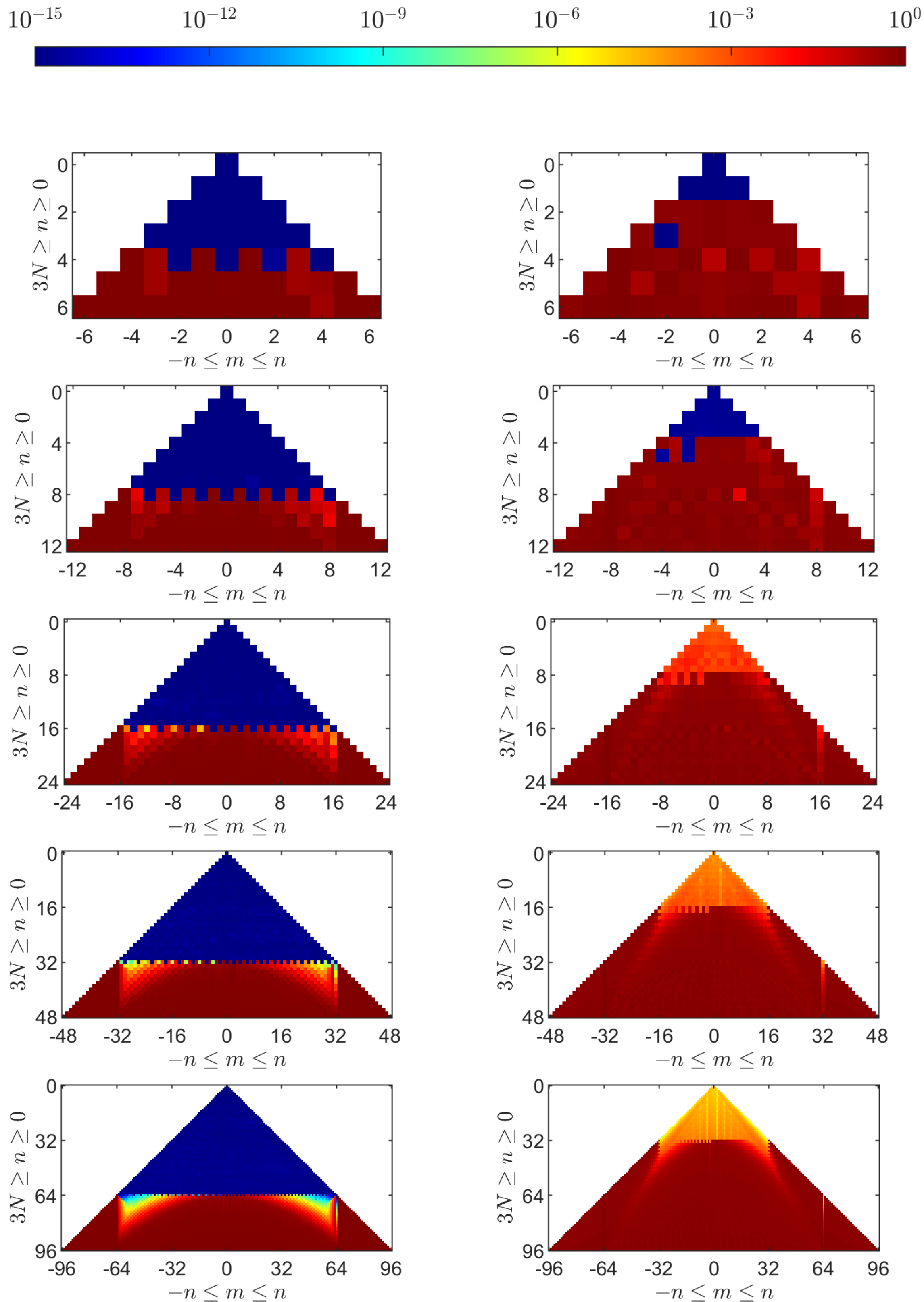

FIGURE 3. Left: distance $d(Y_n^m, \mathcal{Y}'_{3N})$. Right: distance $d(Y_n^m, \mathcal{Y}'_{\mathrm{SVD}})$. From top to bottom: $N = 2$, 4, 8, 16 and 32.

	-6	-5	-4	-3	-2	-1	0	1	2	3	4	5	6
0							0						
1						0	4.7e-17	4.7e-17					
2					0	6.2e-16	7.6e-17	2.3e-16	3.5e-16				
3				2.2e-16	7.7e-17	2.2e-16	3.3e-16	3.6e-16	4.9e-16	3.2e-16			
4			1	0.35	5.1e-16	0.94	4.8e-16	0.94	1.6e-15	0.35	9.3e-16		
5		0.99	1	0.32	1	0.96	0.89	0.96	1	0.32	0.45	0.99	
6	1	1	1	1	1	1	0.94	1	1	1	0.35	1	1

TABLE 2. Distance $d(Y_n^m, \mathcal{Y}'_{3N}) = \|Y_n^m - \Pi_{\mathcal{U}_N} Y_n^m\|_2$, $0 \le n \le 3N$, $-n \le m \le n$; $N = 2$.

	-6	-5	-4	-3	-2	-1	0	1	2	3	4	5	6
0							8.3e-16						
1						9.9e-16	8.3e-16	1.2e-15					
2					0.68	0.68	0.74	0.68	0.74				
3				0.71	1.1e-15	0.68	0.75	0.68	0.64	0.71			
4			1	0.75	0.71	0.97	0.15	0.97	0.23	0.75	0.18		
5		0.71	1	0.25	1	0.69	0.59	0.69	0.77	0.25	0.3	0.71	
6	0.71	0.84	1	0.84	0.73	0.79	0.59	0.79	0.9	0.84	0.22	0.84	0.76

TABLE 3. Distance $d(Y_n^m, \mathcal{Y}'_{\mathrm{SVD}}) = \|Y_n^m - \Pi_{\mathcal{U}_{\mathrm{SVD}}} Y_n^m\|_2$, $0 \le n \le 3N$, $-n \le m \le n$; $N = 2$.

	$d(Y_n^m, \mathcal{Y}'_{3N})$							$d(Y_n^m, \mathcal{Y}'_{\mathrm{SVD}})$						
N	min	Q1	median	Q3	max	mean	std	min	Q1	median	Q3	max	mean	std
2	0	3.5e-16	0.35	1	1	0.51	0.47	8.3e-16	0.52	0.71	0.79	1	0.62	0.3
4	0	5.9e-16	0.37	0.99	1	0.46	0.46	1.7e-15	0.52	0.69	0.73	1	0.59	0.27
8	0	8.8e-16	0.1	0.98	1	0.42	0.45	0.00038	0.48	0.68	0.71	1	0.56	0.26
16	0	1.1e-15	0.024	0.93	1	0.4	0.45	3.1e-05	0.48	0.67	0.71	1	0.54	0.26
32	0	1.4e-15	0.0014	0.91	1	0.39	0.44	2.3e-08	0.45	0.66	0.71	1	0.53	0.26

TABLE 4. Comparison statistics of the distances $d(Y_n^m, \mathcal{Y}'_{3N})$ and $d(Y_n^m, \mathcal{Y}'_{\mathrm{SVD}})$, $|m| \le n \le 3N$: minimum, first quartile, median, third quartile, maximum, mean and standard deviation.

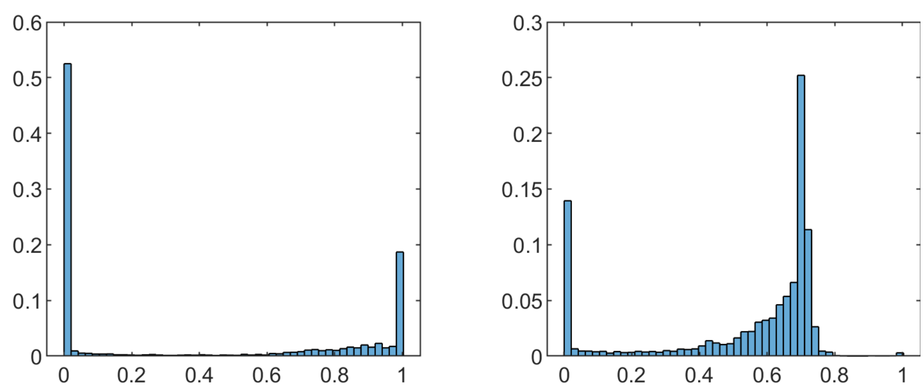

FIGURE 4. Histogram of the distances $d(Y_n^m, \mathcal{Y}'_{3N})$ (left panel) and $d(Y_n^m, \mathcal{Y}'_{\mathrm{SVD}})$ (right panel), with $|m| \le n \le 3N = 3 \cdot 32$.

5.4. **Interpolation test cases.** We interpolate the following set of test functions on the sphere $\boldsymbol{S}^2$.

$$\begin{aligned} f_1(x,y,z) &= 1 + x + y^2 + yx^2 + x^4 + y^5 + x^2y^2z^2, \\ f_2(x,y,z) &= \tfrac{3}{4}\exp\left[-\tfrac{(9x-2)^2}{4} - \tfrac{(9y-2)^2}{4} - \tfrac{(9z-2)^2}{4}\right], \\ &\quad + \tfrac{3}{4}\exp\left[-\tfrac{(9x+1)^2}{49} - \tfrac{9y+1}{10} - \tfrac{9z+1}{10}\right], \\ &\quad + \tfrac{1}{2}\exp\left[-\tfrac{(9x-7)^2}{4} - \tfrac{(9y-3)^2}{4} - \tfrac{(9z-5)^2}{4}\right], \\ &\quad - \tfrac{1}{5}\exp\left[-(9x-4)^2 - (9y-7)^2 - (9z-5)^2\right], \\ f_3(x,y,z) &= \tfrac{1}{9}[1 + \tanh(-9x - 9y + 9z)], \\ f_4(x,y,z) &= \tfrac{1}{9}[1 + \mathrm{sign}(-9x - 9y + 9z)], \end{aligned}$$

The function f_1 is polynomial and $f_1 \in \oplus_{n\le 6} Y_n$. The functions f_2 and f_3 are regular and they have many SH components in their expansion (51). The function f_4 is discontinuous. In Fig. 5, the interpolation errors with $N = 2$ and $N = 4$ for this set of functions is displayed. Furthermore, we display in Fig. 6 the uniform error and the root mean squared error (RMSE) on CS_N.

$$\begin{cases} e_\infty(N, f_i) \triangleq \|f_i|_{\mathrm{CS}_M} - \mathcal{I}_N f_i|_{\mathrm{CS}_M}\|_\infty = \max\limits_{\boldsymbol{x}\in \mathrm{CS}_M} |f_i(\boldsymbol{x}) - (\mathcal{I}_N f_i)(\boldsymbol{x})|, \\ e_2(N, f_i) \triangleq \frac{1}{(\bar{N}_M)^{1/2}} \|f_i|_{\mathrm{CS}_M} - \mathcal{I}_N f_i|_{\mathrm{CS}_N}\|_2 = \left(\frac{1}{\bar{N}}\sum_{\boldsymbol{x}\in\mathrm{CS}_N} |f_i(\boldsymbol{x}) - (\mathcal{I}_N f_i)(\boldsymbol{x})|^2\right)^{1/2}. \end{cases} \tag{58}$$

For N large enough, $f_1 \in \mathcal{Y}'_{3N}$, which gives a null error. The smooth function f_2 is interpolated with an error decreasing with N. This is also the case for the function f_3, with a decreasing rate smaller than the one for f_2. This reflects the C^p regularity of the functions f_2 and f_3. Finally, as expected, the discontinuous function f_4 is not well interpolated. The RMSE decreases very slowly, and the uniform error does not decrease.

5.5. **Poisson problem on the sphere.** Let $g : \boldsymbol{x} \in \mathbb{S}^2 \mapsto g(\boldsymbol{x})$ a function defined on the sphere. We consider the null mean Poisson equation on the sphere in the class of regular functions (say C^∞):

$$\begin{cases} \Delta u = g \\ \displaystyle\int_{\mathbb{S}^2} u\,d\sigma = 0 \end{cases} \quad \text{on } \mathbb{S}^2. \tag{59}$$

Consider the expansion (51) of g

$$g = \sum_{n\ge 0} \sum_{|m|\le n} g_{n,m} Y_n^m. \tag{60}$$

Then, using that

$$\Delta Y_n^m = -n(n+1)Y_n^m, \tag{61}$$

the solution of (59) is

$$g = -\sum_{n\ge 1}\sum_{|m|\le n} \frac{g_{n,m}}{n(n+1)} Y_n^m. \tag{62}$$

The null mean assumption on u gives that there is no contribution for $n = 0$.

Consider the Cubed-Sphere CS_N. Our numerical scheme to approximate (59) using the space $\mathcal{Y}'_{3N}$ in (48) is to use a spectral like approach as follows.

(1) Define g^*, the restriction of $g(\boldsymbol{x})$ to CS_N by

$$g_j^* = [g(\boldsymbol{x}_j)], \quad j \in [\![1 : \bar{N}]\!] \tag{63}$$

(2) Calculate the SH function $g_h(\boldsymbol{x}) \in \mathcal{Y}'_{3N}$ defined by

$$g_h(\boldsymbol{x}) = \sum \hat{g}_n^m Y_n^m(\boldsymbol{x}) \tag{64}$$

where the vector $\hat{g} \in \mathbf{R}^{\bar{N}}$ is given by $\hat{g} = \tilde{\boldsymbol{U}}_{3N}(\boldsymbol{L}_{3N}^\intercal)^{-1}\boldsymbol{V}_{3N}^\intercal g|_{\mathrm{CS}_N}$

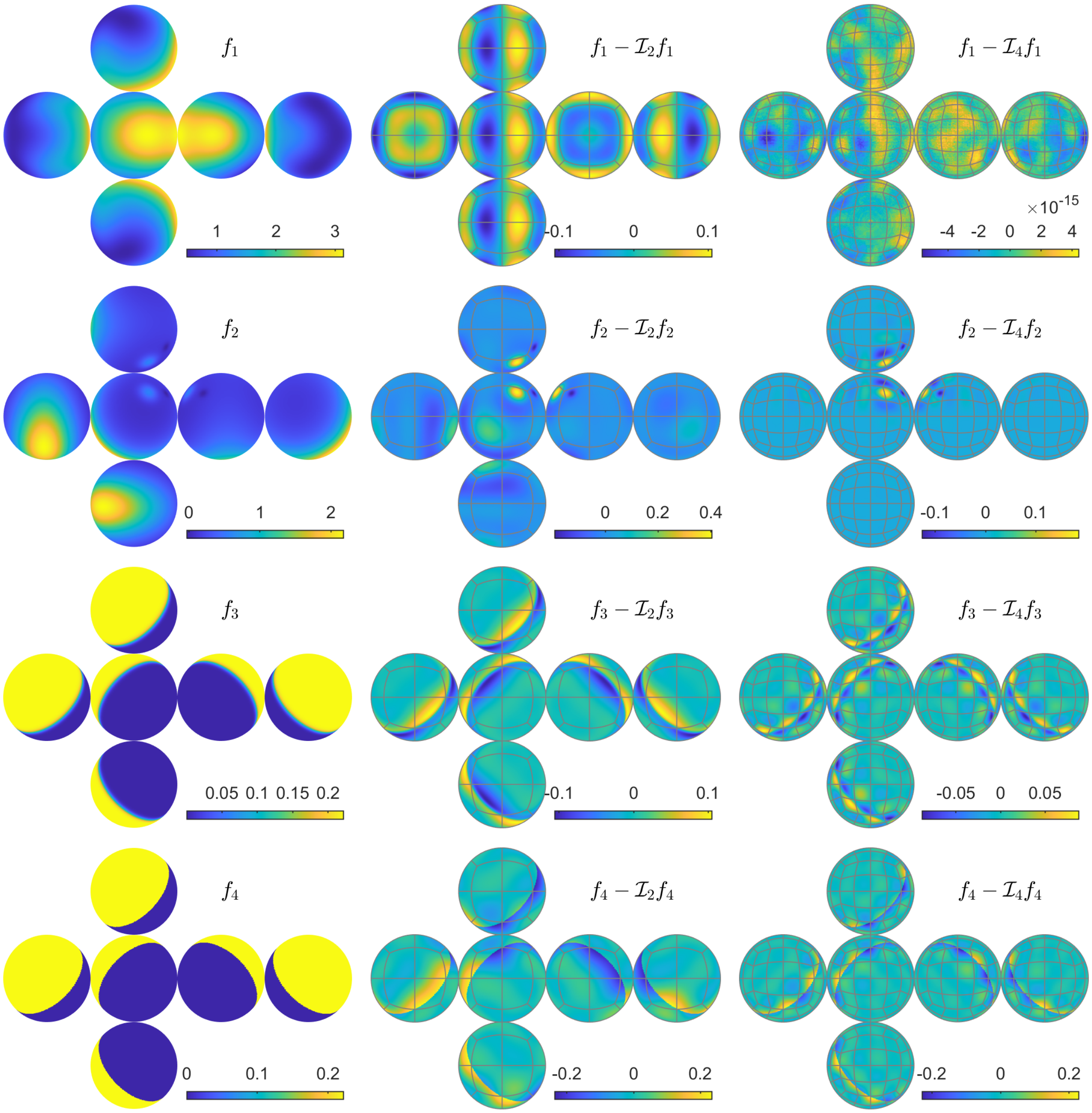

FIGURE 5. Interpolation of test functions. Left: test functions. Middle, right: interpolation error on CS_2, CS_4.

(3) Define $\hat{u} \in \mathbf{R}^{\bar{N}}$ by $\hat{u} = \Lambda \hat{g}$ where Λ is the diagonal matrix

$$\Lambda = \begin{bmatrix} \Lambda^{(0)} & & & \\ & \Lambda^{(1)} & (0) & \\ & (0) & \ddots & \\ & & & \Lambda^{(3N)} \end{bmatrix} \in \mathbb{R}^{\bar{N}\times\bar{N}}, \text{ and } \Lambda^{(n)}_{i,i} = \begin{cases} 0 & \text{if } n = 0 \\ -\frac{1}{n(n+1)} & \text{else.} \end{cases} \quad -n \le i \le n$$

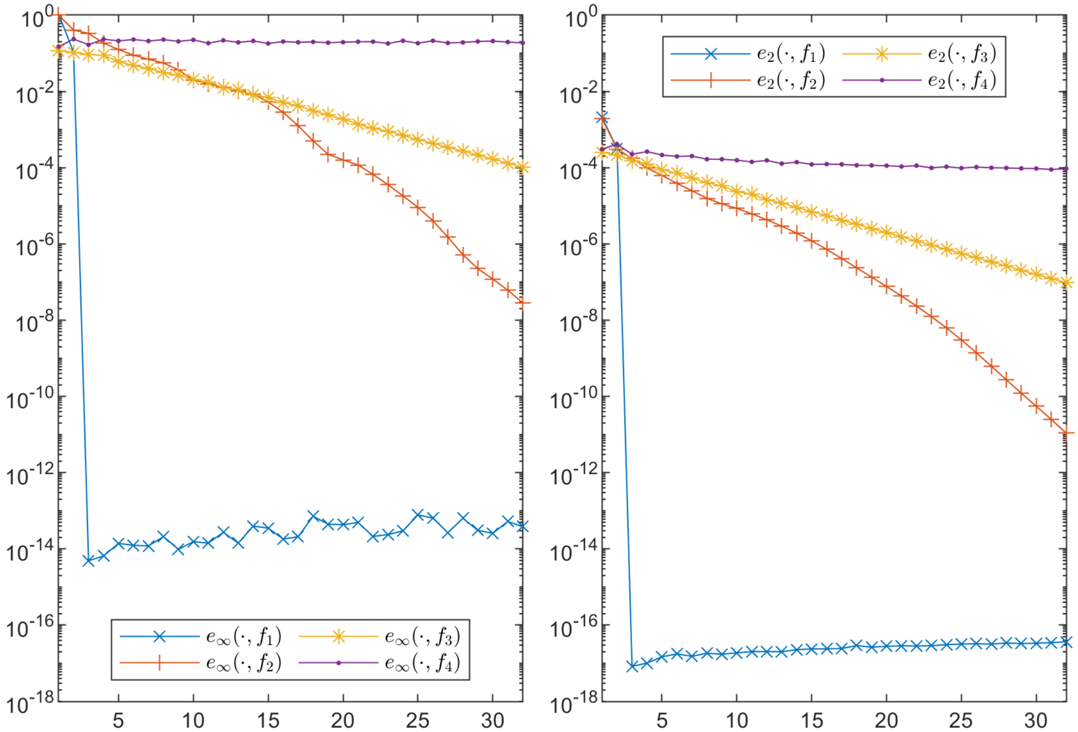

FIGURE 6. Interpolation error (log 10-scale) of test functions on CS_N, for $1 \leq N \leq 32$. Any error is evaluated on CS_{65}. Left: uniform error; right: RMSE.

(4) Define $u_h(\boldsymbol{x})$ by

$$u_h(\boldsymbol{x}) = \sum \hat{u}_n^m Y_n^m(\boldsymbol{x}) \tag{65}$$

(5) Evaluate u_h^*, the restriction to the CS_N of $u_h(\boldsymbol{x})$.

Selecting $\Lambda_{0,0}^{(0)} = 0$ emplies that $\displaystyle\int_{\mathbb{S}^2} u_h d\sigma = 0$ at the discrete level. Second, according to Corollary 4.10, we have $u_h = u$ in the case where $g \in \mathcal{Y}'_{3N}$.

We consider the test case in [4, 14]. Let $g = g_a + g_b$ given in longitude-latitude coordinate (λ, θ) where

$$\begin{cases} g_a(\lambda,\theta) = -(m+1)(m+2)\sin(\theta)\cos^m(\theta)\cos(m(\lambda - d_m)) \\ g_b(\lambda,\theta) = m(m+1)\cos^m(\theta)\cos(m(\lambda - e_m)). \end{cases} \tag{66}$$

The exact solution is $u = u_a + u_b$ with

$$\begin{cases} u_a(\lambda,\theta) = \begin{cases} -\sin(\theta)\cos^m(\theta)\cos(m(\lambda - d_m)) & \text{if } m > 0 \\ -\sin(\theta) - 1 & \text{if } m = 0 \end{cases} \\ u_b(\lambda,\theta) = \cos^m(\theta)\cos(m(\lambda - e_m)). \end{cases} \tag{67}$$

In the sequel, the values e_m and d_m are phase angles in $[0, 2\pi]$ picked at random.

The accuracy is evaluated by

$$E = \sqrt{\frac{\displaystyle\sum_{\boldsymbol{x}_j \in \mathrm{CS}_N} |u_h(\boldsymbol{x}_j) - u(\boldsymbol{x}_i)|^2}{\displaystyle\sum_{\boldsymbol{x}_j \in \mathrm{CS}_N} |u(\boldsymbol{x}_j)|^2}} \tag{68}$$

This evaluation is repeated for 30 values of e_m and d_m in $[0, 2\pi]$ (picked randomly). Fig 7 reports the mean value of $\log_{10}(E)$ in function of m. Three Cubed Spheres are considered, CS_8, CS_{16} and CS_{32}. For a given

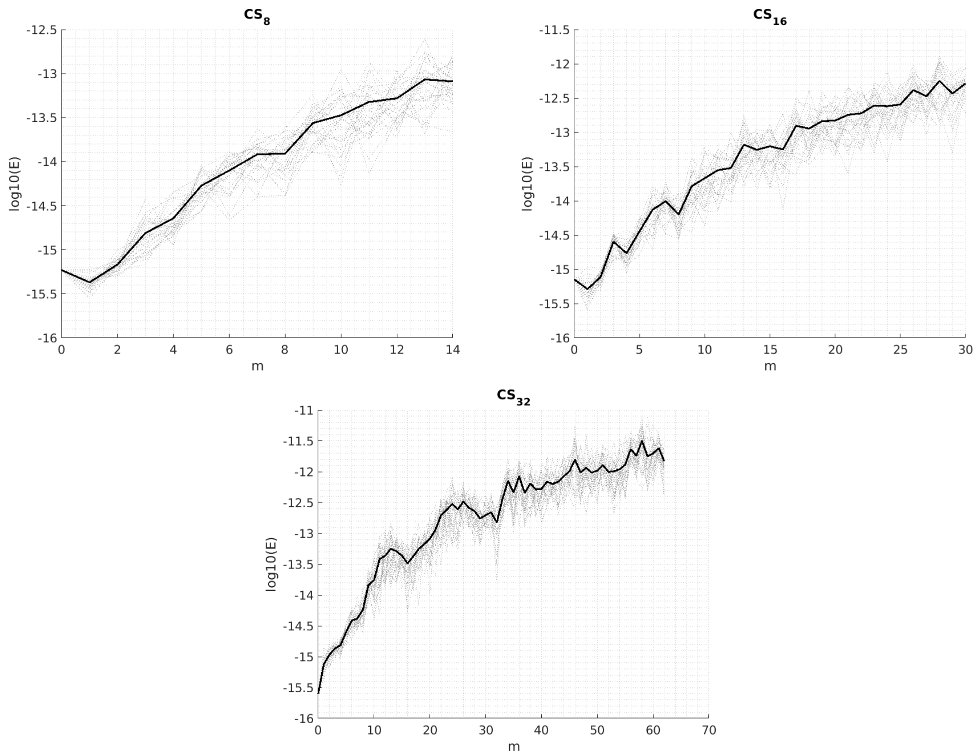

FIGURE 7. Poisson equation solver error on CS_N for $N \in \{8, 16, 32\}$. The relative error is plotted related to the value m for 30 random values e_m and d_m in $[0, 2\pi]$.

grid CS_N, the error E increases with m, which is expected, due to the cut-off in resolution of the grid. The magnitude of the error E is similar to the one reported in [4] which uses a standard collocation spectral solver with a lon-lat grid. Here, there is no loss in accuracy, despite that the function (67) is expressed in lon-lat coordinates. The truncation reported in Section 5.2 is analyzed as follows. In Table 5 the error E is reported for $m \in \{2N-1, 2N, 2N+1\}$. Consider for example CS_{16}. For $m = 2N - 1$, the error is of the order of 10^{-13}. For $m = 2N$, the error is augmented by a factor of 10^5, which gives $E \simeq 10^{-6}$. Finally, another augmentation by the same factor of 10^5 occurs again leading to $E \simeq 10^{-1}$ for $m = 2N + 1$. This corresponds to an undersampling of the function g along the equator.

	$m = 2N-1$	$m = 2N$	$m = 2N+1$
$N = 8$	4.53×10^{-9}	3.25×10^{-4}	2.74×10^{-1}
$N = 16$	3.31×10^{-13}	2.96×10^{-6}	1.31×10^{-1}
$N = 32$	1.91×10^{-12}	1.33×10^{-9}	6.40×10^{-2}

TABLE 5. Poisson equation error on CS_N for $N \in \{8, 16, 32\}$. The relative error E in (68) is related to the value m. It is averaged over 30 random values e_m and d_m in $[0, 2\pi]$.

6. Conclusion

In this study, a methodology to associate a Spherical Harmonics subspace to the Cubed Sphere CS_N has been introduced. The particular subspace considered in Section 4 is based on a specific Column Echelon factorisation of the Vandermonde matrix. This space seems promising in terms of approximation power. As seen in Section 5.2, it compares favourably to alternatives factorisations, such as the SVD.

This work took its origin in the numerical observation of the rank increment property stated in Claim 5.1. A proof of this claim, which is not available at time, is an objective of further studies. Applying the new interpolation procedure to various contexts is also an objective. First, spherical quadrature rules will be addressed elsewhere. Another issue is the symmetry properties of the interpolation space. In particular, its invariance under the action of the group of the sphere, has to be undertaken, [2]. Computational issues clearly require further analysis. A preliminary report is presented in Appendix A (condition number of the Vandermonde matrix and run time to evaluate the SH basis).

Finally, an important goal is the application of this new framework to PDE's in meteorology, in the spirit of the approach in Section 5.5.

Appendix A. Computational issues

We report in Table 6, some data related to the computation of the Vandermonde matrix $\boldsymbol{A}_{3N}$ in (22) and of the lower triangular matrix $\boldsymbol{L}_{3N}$ in (38). In the last line, the run time measured using a sequential matlab code is also reported. Small values of the condition number are observed in both cases; for example, for

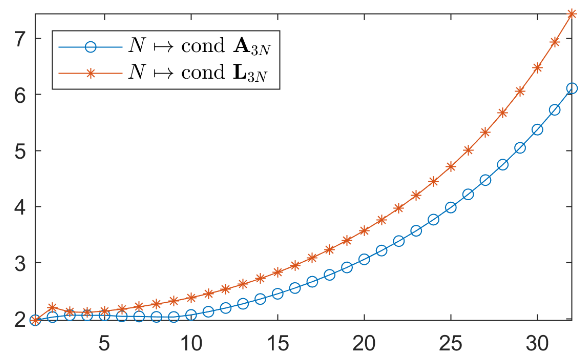

Figure 8. Condition number of the matrices $\boldsymbol{A}_{3N}$ and $\boldsymbol{L}_{3N}$ for $1 \leq N \leq 32$.

N	1	2	4	8	16	32
$\bar{N} = 6N^2 + 2$	8	26	98	386	1538	6146
cond $\boldsymbol{A}_{3N}$	2	2	2.1	2	2.5	6.1
cond $\boldsymbol{L}_{3N}$	2	2.2	2.1	2.3	3	7.4
CPU time (s)	8.8e-03	1.7e-03	6.7e-03	1.1e-01	4.7e+00	3.0e+02

Table 6. Condition number of the matrices$\boldsymbol{A}_{3N}$ and $\boldsymbol{L}_{3N}$. The CPU time is reported on the third line.

$N = 32$, the number of grid points is $\bar{N} = 6146$, and cond $\boldsymbol{L}_{3N} = 7.4$. As a result, for moderate values of $\bar{N}$, we expect an accurate evaluation of the interpolating functions. By the way, the behaviors of the condition numbers as N grows look similar. This numerically shows that the unisolvent space $\mathcal{Y}'_{3N}$ almost captures the condition number of the full VDM matrix $\boldsymbol{A}_{3N}$.

The reported CPU time corresponds to the computation of the matrix $\boldsymbol{L}_{3N}$, of the full basis U_k of Y_k, $0 \leq k \leq 3N$, and of the orthogonal matrix $\boldsymbol{V}_{3N}$. It also includes assembling the matrices A_k, $k \leq 3N$. [1] For each value $N = 1, 2, 4, 8, 16, 32$, the computations are repeated five times and the reported CPU time is the average.

[1]Matlab code on a Laptop using a CPU Intel i9-9880H@2.30 GHz.

Appendix B. Representation of the basis functions for $N = 2$

For completeness, we report the computed basis for $N = 2$. Fig. 9 reports the basis of the subspace $\mathcal{Y}_6'$ and Fig. 10 reports the basis of the of the orthogonal set $(\mathcal{Y}_6')^{\perp}$. For each basis function u, the convention is the following: we plot u on the sphere, and we draw the CS_2 mesh; then we represent six views of this sphere, taken in front of the six panels of the cubed sphere.

References

[1] K. Atkinson and W. Han. *Spherical Harmonics and Approximations on the Unit Sphere: an introduction*. Number 2044 in Lect. Notes. Math. Springer-Verlag, 2012.

[2] J.-B. Bellet. Symmetry group of the equiangular cubed sphere. `hal-03071135`, 2020.

[3] M. Brachet and J.-P. Croisille. Spherical Shallow Water simulation by a cubed sphere finite difference solver. *Quat. Jour. Roy. Met. Soc.*, 2021.

[4] H-B. Cheong. Double fourier series on a sphere: applications to elliptic and vorticity equations. *J. Comp. Phys.*, 157:327–349, 2000.

[5] R. Daley and Y. Bourassa. Rhomboidal versus triangular spherical harmonic truncation:some verification statistics. *Atmosphere-Ocean*, 16(2):187–196, 2010.

[6] G.H. Golub and C.F. Van Loan. *Matrix Computations*. John Hopkins University Press, 3-rd edition, 1996.

[7] M. N. Jones. *Spherical Harmonics and Tensors for classical field theory*. Research Studies Press, 1985.

[8] S. Kunis, H.M. Möller, and U. von der Ohe. Prony's method on the sphere. *SMAI J. of Comp. Math.*, S5:87–97, 2019.

[9] R.D Nair, S. J. Thomas, and R. D. Loft. A discontinuous galerkin transport scheme on the cubed sphere. *Month Weath. Rev.*, 133(4):814–828, 04 2005.

[10] B. Portelenelle and J.-P. Croisille. An efficient quadrature rule on the cubed sphere. *J. Comp. App. Math.*, 328:59–74, 2018.

[11] R.J. Purser and M. Rancic. Smooth quasi-homogeneous gridding of the sphere. *J. Comput. Phys.*, 124:637–647, 1998.

[12] C. Ronchi, R. Iacono, and P. S. Paolucci. The Cubed Sphere: A new method for the solution of partial differential equations in spherical geometry. *J. Comput. Phys.*, 124:93–114, 1996.

[13] P. A. Ullrich, C. Jablonowski, and B. van Leer. High order finite-volume methods for the shallow-water equations on the sphere. *J. Comput. Phys.*, 229:6104–6134, 2010.

[14] Y.K. Yee. Solution of Poisson's equation on a sphere by truncated double Fourier series. *Mon. Weath. Rev.*, 109:501–501, 1981.

† Université de Lorraine, CNRS, IECL, F-57000 Metz, France
Email address: jean-baptiste.bellet@univ-lorraine.fr, jean-pierre.croisille@univ-lorraine.fr

‡ Université de Poitiers, CNRS, LMA, F-86000 Poitiers, France
Email address: matthieu.brachet@math.univ-poitiers.fr

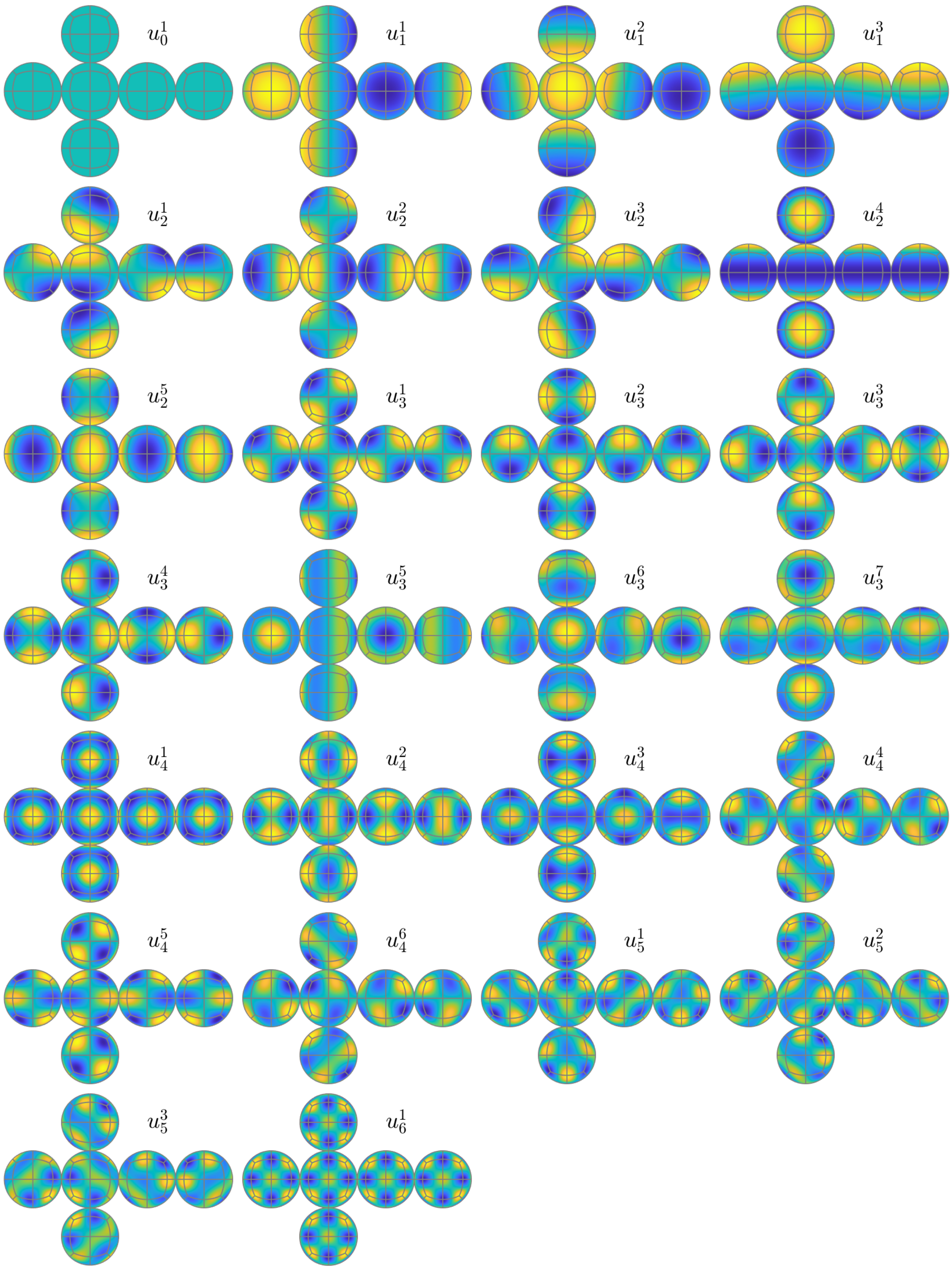

FIGURE 9. Orthonormal basis $u_n^i \in Y_n' \subset Y_n, 1 \leq i \leq g_n, 0 \leq n \leq 3N$, of the unisolvent set $\mathcal{Y}_{3N}' = \oplus_{0 \leq n \leq 3N} Y_n'$; $N = 2$.

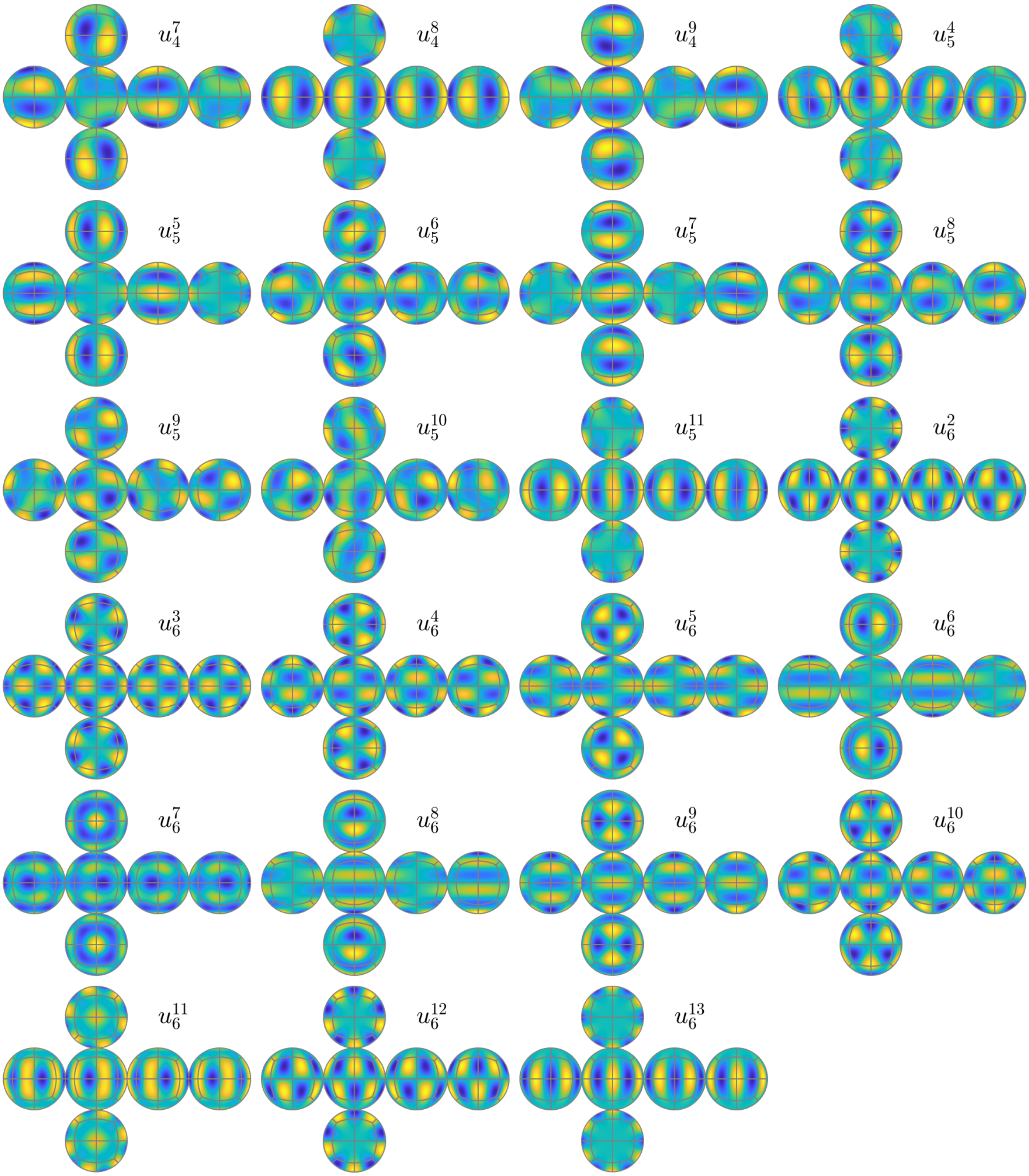

FIGURE 10. Orthonormal basis $u_n^i \in Y_n'', g_n + 1 \leq i \leq 2n+1, 2N \leq n \leq 3N$, of the orthogonal supplementary $\mathcal{Y}_N^{\perp} = \oplus_{2N \leq n \leq 3N} Y_n''$; $N = 2$.